AIAA JOURNAL
Vol. 31, No. 7, July 1993

High-Speed Turbulence Modeling of Shock-Wave/ Boundary-Layer Interaction

F. Grasso* and D. Falconi†
Università di Roma "La Sapienza", Rome 00184, Italy

In the present paper some of the recent theoretical developments in compressible turbulence modeling are analyzed, and a model that accounts for compressibility and low Reynolds-number effects is developed. The leading compressibility terms have been identified in the dilatation-dissipation, pressure-dilatation, and the scalar product of the Favre velocity and mean pressure gradient. For the dilatation-dissipation a model similar to that of Zeman has been assumed; the pressure-dilatation is modeled according to Sarkar's model; and the "Favre" contribution has been modeled with a gradient law. The model also accounts for compressibility effects on the von Kármán's constant and on the turbulence length scale, which affects the heating rates. A study of hypersonic boundary-layer flows and shock-wave/boundary-layer interactions shows that the effects of compressibility depend on the flow complexity.

Introduction

SHOCK-WAVE turbulent boundary-layer interaction is one of the most challenging problems in hypersonic flows. This flowfield configuration is of practical importance in air-breathing inlets, wing-body junctures, and deflected control surfaces. The successful prediction in computing heating rates, the onset, and the extent of separation for complex flows is a critical issue in the design process to assess vehicle performance and heat-protection systems.

Recently, an improvement in the development of compressible turbulence modeling has been possible for the availability of both high-speed experimental data and direct numerical simulation results (DNS).[1] DNS is helpful in the understanding of physical phenomena. However, it is computationally expensive and it is limited to rather low Reynolds numbers, due to the present limitations in computer technologies. Hence, all scientific and engineering calculations of complex flows at high Mach numbers and high Reynolds numbers require some modeling.

Turbulence models for high-speed flows are generally based on simple variable-density extensions of their incompressible forms, under the assumption of solenoidal fluctuating velocity field. This approach is questionable at high Mach numbers. Indeed, not very satisfactory results are obtained even in simple flows such as boundary layers over flat plate with surface heating. This is mainly due to the increase in density fluctuations with the Mach number that are responsible for changes in the turbulent structures. Although it is difficult to identify and quantify the primary causes of these changes, it has been observed that some additional correlations play a fundamental role in compressible turbulent flows, and their contribution should be taken into account in developing turbulence models for hypersonic flows. The pressure-dilatation term and the dilatation-dissipation (ϵ_d) are the leading compressible effects that contribute to the reduction of the turbulence kinetic energy, and cannot be neglected as recently shown by Sarkar,[2,3] Zeman,[4] and Speziale and Sarkar.[5]

Received April 14, 1992; revision received Nov. 10, 1992; accepted for publication Nov. 11, 1992; presented as Paper 93-0778 at the AIAA 31st Aerospace Sciences Meeting, Reno, NV, Jan. 11-14, 1993.

*Associate Professor, Dipartimento di Meccanica e Aeronautica, Via Eudossiana 18. Member AIAA.
†Graduate Student, Dipartimento di Meccanica e Aeronautica, Via Eudossiana 18.

Another critical issue in developing turbulence models is their ability to predict wall effects. Most of the models developed so far have been moderately successful in computing a variety of engineering problems, mainly for high-Reynolds-number flows. In general, they use wall functions,[6] thus eliminating numerical stiffness, and allow the use of rather coarse grids. However, this approach is not rigorously valid in the presence of 1) strong streamline curvature; 2) adverse pressure gradients; 3) flows where wall transport is needed; 4) separated flows, etc. In all of these cases, the models require a consistent asymptotic behavior at the wall.[7-12] In particular, in the near wall region low Reynolds effects have to be taken into account.

Different degrees of complexities exist in turbulence models for high-speed flows, and they can be classified in zero-, one-, and two-equation models, Reynolds stress closure models, large eddy simulation, etc. In the present work, we deal with two-equation models, which are a good compromise between low- and high-order models, and require limited computational resources and are very attractive from an engineering point of view. The most widely used two-equation models are the k-ϵ and k-ω ones. As shown by Speziale et al.,[8] if one defines the ω as the ratio of ϵ over k, the ω equation is inconsistent unless a cross-diffusion term is added. The k-ω model has been originally developed by Wilcox[13] and solves the governing transport equations for the turbulence kinetic energy (k) and for the vorticity of the energy containing eddies (ω). Wilcox has used the model for high-speed flows by simply adding a compressibility term to account for both pressure-dilatation and dilatation-dissipation. In particular, he has tested both the models developed by Zeman and Sarkar. The former defines the dilatational contributions via an exponential turbulent Mach-number dependency. The latter defines the dilatational terms by a turbulent Mach-number power-law dependency. Wilcox has applied the models to shear layers, and finds that Zeman's predicts somewhat larger spreading rates. Viegas and Rubesin[14] have made a comparative study of several compressibility corrections to turbulence models for high-speed mixing layers. They have concluded that Zeman's model represents the data better than Sarkar's and the standard k-ϵ model. Zhang et al.[11] have analyzed a compressible k-ϵ model that uses Sarkar's model for the dilatational terms and it is asymptotically consistent in the near wall regions. Applications to high-Mach-number flows over a flat plate seem to indicate that in the absence of adverse pressure gradients, asymptotic consistency is more important than compressibility effects. Coakley and Huang[15] have recently investigated several two-equation turbulence models with compressibility cor-

rections for flows over flat plates and complex shock-wave/boundary-layer interaction over ramps. They have concluded that none of the models investigated is able to accurately predict complex flows, even though adequate predictions of flat-plate flows can be obtained. Horstman[16] has studied the use of a two-layer k-ϵ model, originally developed by Rodi[27] for low speeds, and a k-ϵ model modified by Viegas and Rubesin.[14] He has proposed to limit the length scale and the turbulence kinetic energy to reduce the large overshoot in heat transfer rates near reattachment. Applications to two- and three-dimensional shock-wave/boundary-layer interaction problems show reasonable agreement with experiments, even though detailed measurements of fluctuating quantities are lacking. Grasso and Speziale[17] have developed a compressible k-ϵ model whereby the pressure-dilatation and the so-called "Favre" contribution (related to the scalar product of Favre velocity fluctuation and mean pressure gradient) have been defined in terms of the average dilatation, and the dilatation-dissipation has been neglected. However, the model is limited to statistically steady turbulent flows and does not account for low Reynolds effects.

In the present work, we have developed a model that is asymptotically consistent in the near wall region and it accounts for the compressibility effects. In particular, for the dilatation-dissipation a model similar to that of Zeman[4] has been assumed; the pressure-dilatation is modeled according to Sarkar's model.[3] An additional term due to the scalar product of the Favre velocity and the pressure gradient has been found to play an important role in shock-wave/boundary-layer interaction problems and has been modeled with a gradient law.

To assess the ability of the model to correctly predict turbulent high-speed flows, extensive comparisons with experimental data of hypersonic flow over a flat plate with surface heating and over compression ramps are reported.

Governing Equations

The governing equations are the Navier-Stokes equations reformulated for the mean flow variables after introducing a Reynolds decomposition. Both Favre and conventional time averages have been used. In particular, the Favre average ($\tilde{}$) is adopted for the total energy and the velocity field, while the time average ($\bar{}$) is employed for the pressure and the density. The equations are

$$\frac{\partial \bar{\rho}}{\partial t} + \frac{\partial}{\partial x_j}(\bar{\rho}\tilde{u}_j) = 0 \tag{1a}$$

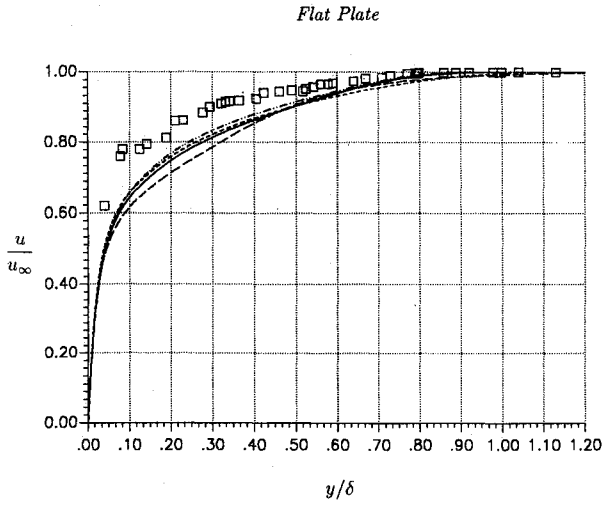

Fig. 1 Velocity distribution vs y/δ (□, Ref. 22; - · ·, compressible 256 × 128; —, compressible 256 × 64; - - -, incompressible 256 × 64; - - -, compressible 128 × 32).

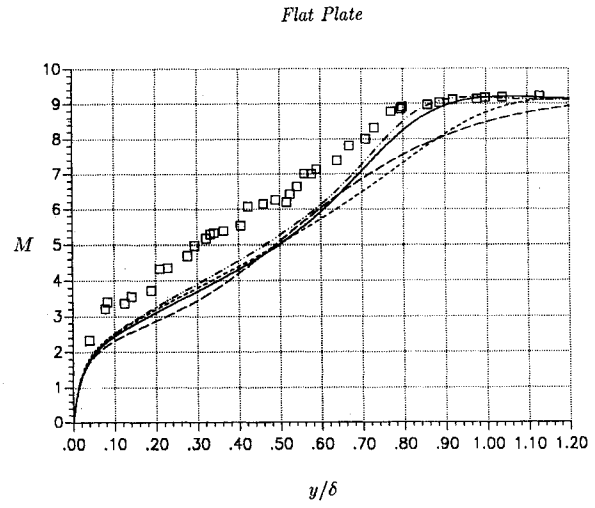

Fig. 2 Mach-number distribution vs y/δ (□, Ref. 22; - · ·, compressible 256 × 128; —, compressible 256 × 64; - - -, incompressible 256 × 64; - - -, compressible 128 × 32).

$$\frac{\partial}{\partial t}(\bar{\rho}\tilde{u}_i) + \frac{\partial}{\partial x_j}[\rho\tilde{u}_i\tilde{u}_j + \bar{p}\delta_{ij} - \sigma_{ij}) = 0 \tag{1b}$$

$$\frac{\partial}{\partial t}(\bar{\rho}\tilde{E}) + \frac{\partial}{\partial x_j}[\bar{\rho}\tilde{E}\tilde{u}_j + \tilde{u}_i(\bar{p}\delta_{ij} - \sigma_{ij}) + q_j] = 0 \tag{1c}$$

where $\bar{\rho}$, $\tilde{u}_i$, and $\tilde{E}$ are, respectively, the density, the Cartesian velocity component, and the total energy per unit mass defined as

$$\tilde{E} = \tilde{e} + \frac{\tilde{u}_i\tilde{u}_i}{2} + \frac{\widetilde{u_i''u_i''}}{2} \tag{2}$$

where $\tilde{e}$ is the Favre-averaged internal energy, and the double prime stands for Favre fluctuation. The pressure is defined according to the equation of state

$$\bar{p} = (\gamma - 1)\bar{\rho}\left[\tilde{E} - \frac{\tilde{u}_i\tilde{u}_i}{2} - \frac{\widetilde{u_i''u_i''}}{2}\right] \tag{3}$$

where γ is the specific heat ratio that is assumed to be constant and equal to 1.4.

The variables σ_{ij} and q_j are, respectively, the total stress tensor and the heat flux vector:

$$\sigma_{ij} = \sigma_{ij}^t + \sigma_{ij}^\ell \tag{4}$$

$$q_j = q_j^t + q_j^\ell \tag{5}$$

The constitutive equations for the laminar contributions are

$$\sigma_{ij}^\ell = 2\bar{\mu}\tilde{S}_{ij} - \tfrac{2}{3}\bar{\mu}\tilde{S}_{ll}\delta_{ij} \tag{6}$$

$$q_j^\ell = -\gamma\frac{\bar{\mu}}{Pr}\frac{\partial\tilde{e}}{\partial x_j} \tag{7}$$

where $\tilde{S}_{ij}$ is the symmetric part of the mean strain tensor, Pr is the Prandtl number, and the molecular viscosity $\bar{\mu}$ is defined through the semiempirical Sutherland's law. The constitutive equations for the turbulent contributions are

$$\sigma_{ij}^t = 2\mu^t\tilde{S}_{ij} - \tfrac{2}{3}[\mu^t\tilde{S}_{ll} + \bar{\rho}k]\,\delta_{ij} \tag{8}$$

$$q_j^t = -\gamma\frac{\mu^t}{Pr_t}\frac{\partial\tilde{e}}{\partial x_j} \tag{9}$$

where μ^t, k, and Pr_t are, respectively, the turbulent viscosity, the turbulence kinetic energy, and the turbulent Prandtl number. In the present work, a constant turbulent Prandtl number

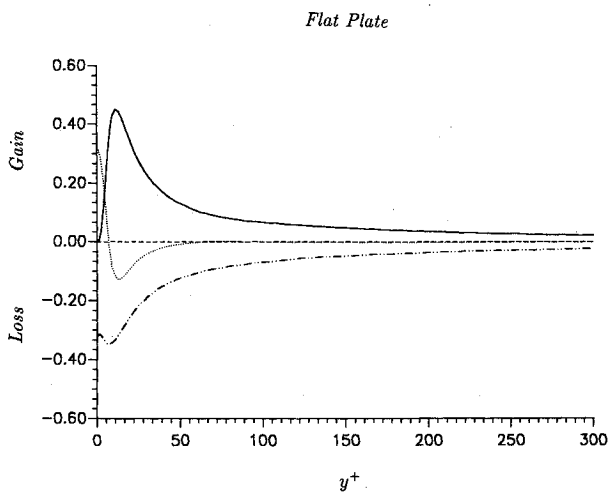

Fig. 3 Turbulence kinetic energy budget vs y^+, incompressible (—, P_k; - · -, ϵ; · · ·, Diff.; - - -, Conv.).

is used, which is a rather strong approximation expecially in the presence of complex flows.[18] The turbulent viscosity is defined in terms of the turbulence kinetic energy and the solenoidal dissipation (ϵ), whose model equations are given in the next section.

For the sake of clarity in all subsequent sections, the ($\bar{}$) and ($\tilde{}$) are dropped, unless confusion arises.

Two-Equation Compressible Model

In the present work, a two-equation k-ϵ model of turbulence is developed that accounts for compressibility and low Reynolds effects. The leading terms responsible for the compressibility effects are found to be the trace of the pressure-strain tensor, the scalar product of the mean pressure gradient with the Favre-averaged velocity fluctuation, and the dilatation-dissipation. All terms play a strong role in highspeed adverse pressure gradient flows and cannot be disregarded.

The model is developed for complex flows which are characterized by strong streamwise curvature, adverse pressure gradients, separated flows, etc. Therefore, the model equations must satisfy the asymptotic consistency, i.e., the near wall behavior of turbulent quantities.[7-12] By assuming that the velocity, pressure, and density fluctuations vanish at the wall, the enforcement of the asymptotic behavior leads to:

$$\frac{\partial \rho k}{\partial t} + \frac{\partial \rho u_j k}{\partial x_j} = \frac{\partial}{\partial x_j}\left[\left(\mu + \frac{\mu^t}{\sigma_k}\right)\frac{\partial k}{\partial x_j}\right] + P_k - \rho\epsilon + \Pi_{c,1} + \Pi_{c,2} + \Pi_{c,3} \tag{10}$$

$$\frac{\partial \rho \epsilon}{\partial t} + \frac{\partial \rho u_j \epsilon}{\partial x_j} = \frac{\partial}{\partial x_j}\left[\left(\mu + \frac{\mu^t}{\sigma_\epsilon}\right)\frac{\partial \epsilon}{\partial x_j}\right] + P_\epsilon - \Phi_\epsilon \tag{11}$$

where P_k, P_ϵ, Φ_ϵ, and $\Pi_{c,i}$ represent, respectively, the production of the turbulence kinetic energy, the production and the dissipation of the solenoidal dissipation, and the compressibility effects, defined as

$$P_k = [2\mu^t S_{ij} - \tfrac{2}{3}\mu^t S_{ll}\delta_{ij} - \tfrac{2}{3}\rho k \delta_{ij}]S_{ij}, \qquad P_\epsilon = C_{\epsilon 1}(\epsilon/k)P_k$$

$$\Phi_\epsilon = C_{\epsilon 2} f_2 \rho(\epsilon^2/k), \qquad \Pi_{c,1} = \overline{p' u'_{i,i}}, \qquad \Pi_{c,2} = \frac{\overline{\rho' u'_i}}{\rho}\frac{\partial p}{\partial x_i}$$

$$\Pi_{c,3} = -\rho[\tfrac{4}{3}(\nu \overline{S'_{ll} S'_{ll}})]$$

and $k = \frac{1}{2}\,\overline{\rho u'_i u'_i}/\rho$.

The turbulent viscosity is defined as

$$\mu^t = C_\mu f_\mu \rho(k^2/\epsilon) \tag{12}$$

where $C_\mu = 0.09$. Near the wall f_μ is a function of $\mathcal{O}(1/y^+)$ and f_2 is a function of $\mathcal{O}(y^{+2})$ (y^+ is the viscous coordinate defined as $y^+ = u_\tau y/\nu_w$). Following the work of Speziale et al.[8], we have used the following expressions for f_μ and f_2:

$$f_\mu = [1 + (3.45/\sqrt{Re_t})]\tanh(y^+/80) \tag{13}$$

$$f_2 = [1 - \exp(-y^+/A)]^2 \tag{14}$$

where $Re_t = k^2/(\nu\epsilon)$ is the turbulent Reynolds number, and the value of $A = 4.9$ (obtained from direct numerical simulation of planar channel flows) has been retained. A turbulence Reynolds-number dependency is assumed for $C_{\epsilon 2}$:[19]

$$C_{\epsilon 2} = 1.83[1 - (2/9)\exp(-Re_t^2/36)] \tag{15}$$

Compressibility Effects

Wilcox[13] has recently shown that compressibility affects the von Kármán's constant (k_v) as well. In particular, he has shown that k_v deviates from the standard value ($\tilde{k}_v = 0.41$), according to the following formula

$$k_v^2 = \tilde{k}_v^2 - [(C_{\epsilon 1} + \tilde{C}_{\epsilon 2})\sigma_\epsilon + \tfrac{1}{2}(\gamma - 1)\frac{Pr_t}{\sigma_k}(3C_{\epsilon 1} - \tilde{C}_{\epsilon 2})\sigma_\epsilon] M_\tau^2 + \ldots \tag{16}$$

where M_τ is a turbulent Mach number defined as $M_\tau = u_\tau/(\gamma R T_w)$ (u_τ is the friction velocity). In the present work, the von Kármán's constant has been determined from the above equation that gives $k_v = 0.37$ by assuming $M_\tau = 0.06$ (typical of high-speed flows), $Pr_t = 0.9$, $C_{\epsilon 1} = 1.60$, $\tilde{C}_{\epsilon 2} = 1.83$, $\sigma_k = 1.55$, and $\sigma_\epsilon = 2$. The turbulent Prandtl number σ_k has been determined from experimentally measured values used to define turbulent viscosity laws in a study on heat transfer for separated flows,[20] which shows that σ_k varies between 1.47 and 1.70. The turbulent Prandtl number σ_ϵ has been determined assuming the same proportionality of the standard values. The constant $C_{\epsilon 1}$ has been obtained from the equilibrium relation.

Pressure-Dilatation

The model is based on the assumption that the pressure fluctuation can be decomposed in an "incompressible" pressure fluctuation (p'_I), and a "compressible" one (p'_C), and that the former contributes to the pressure-dilatation, thus yielding[1,3]

$$\Pi_{c,1} = (-\alpha_2 P_k + \alpha_3 \rho\epsilon)M_t^2 \tag{17}$$

where the turbulent Mach number is defined as $M_t = \sqrt{2k/(\gamma RT)}$, $\alpha_2 = 0.40$, and $\alpha_3 = 0.20$.

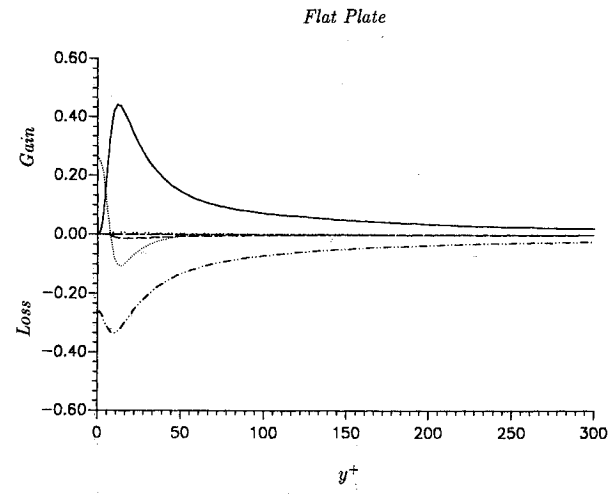

Fig. 4 Turbulence kinetic energy budget vs y^+, compressible (—, P_k; - · -, ϵ; · · ·, $\Pi_{c,1}$; -·-, $\Pi_{c,2}$; - - -, $\Pi_{c,3}$; · · ·, Diff.; - - -, Conv.).

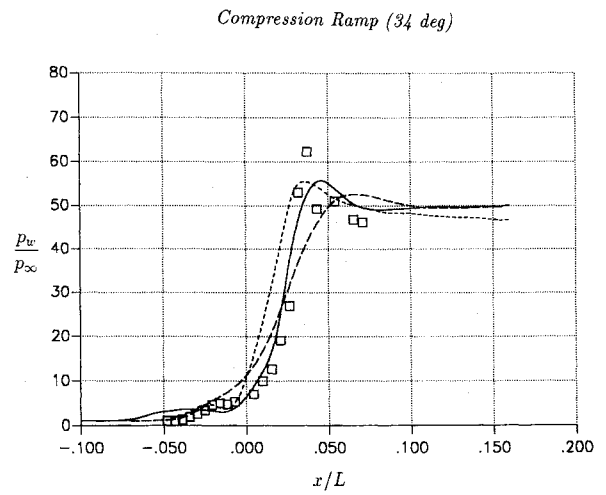

Fig. 5 Surface pressure vs x/L (□, Ref. 22; —, compressible; - - -, incompressible; - - -, incompressible with standard constants).

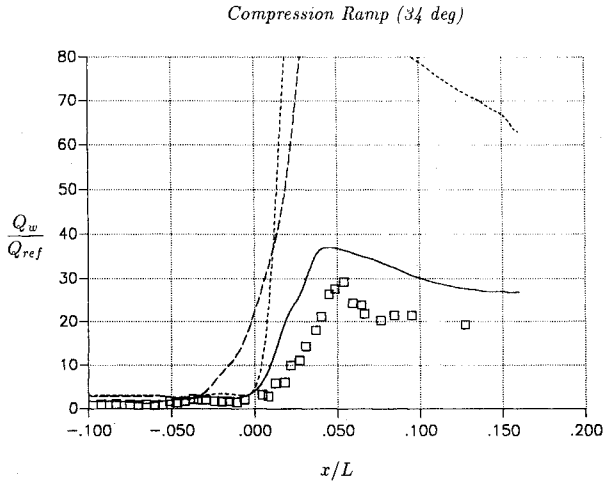

Fig. 6 Surface heat transfer vs x/L (□, Ref 22; —, compressible; - - -, incompressible; - - -, incompressible with standard constants).

Dilatation-Dissipation

The dilatation-dissipation contribution ($\Pi_{c,3}$) has been modeled following closely the work of Zeman,[4] which postulates the existence of shock-like eddy structures, which are embedded within the energy-containing eddies, and which are assumed to be responsible for the dilatational contributions. In particular, Zeman obtains an exponential turbulence Mach-number dependency.

In the original model of Zeman, the term $\Pi_{c,3}$ accounts also for the pressure-dilatation contribution. In the present work, two separate models have been used for the dilatational contributions. Therefore, assuming that the pressure-dilatation and the dilatation-dissipation are of the same order of magnitude,[1] we have reduced the contribution of $\Pi_{c,3}$ approximately by a factor of two. Moreover, as proposed by Wilcox,[13] we have increased the threshold value of the turbulent Mach number below which the dilatation-dissipation is set equal to zero to a value of 0.3 and we obtain

$$\Pi_{c,3} = -0.40\,\rho\epsilon\left\{1 - \exp\left[-\left(\frac{M_t - 0.3}{0.8}\right)^2\right]\right\} \qquad (18)$$

Favre-Velocity Contribution

High-speed flows are generally characterized by large pressure gradients. Consequently, the contribution due to the scalar product of the Favre-velocity and the mean pressure gradient may be important. In the present work, a gradient law is assumed

$$\Pi_{c,2} = -\frac{\mu^t}{\rho^2}\frac{1}{\sigma_\rho}\frac{\partial \rho}{\partial x_j}\frac{\partial p}{\partial x_j} \qquad (19)$$

where a constant value of the turbulent Prandtl number σ_ρ is assumed ($\sigma_\rho = 0.5$).[5]

Turbulent Length Scale Correction

As observed by Marvin and Coakley,[21] wall pressure predictions are improved by accounting for compressibility effects. However, the peak heating is rather unaffected and it is generally overpredicted. To overcome such a deficiency, they introduce an upper bound on the turbulent length scale, and redefine the turbulent viscosity as follows

$$\mu^t = C_\mu f_\mu \rho \ell_m k^{1/2} \qquad (20)$$

$$\ell_m = \min\left(C_\ell y, \frac{k^{3/2}}{\epsilon}\right) \qquad (21)$$

where y is the distance from the wall, and C_ℓ depends on the von Kármán's constant. Horstman[16] and Marvin and Coakley[21] do not account for compressibility corrections on k_v and use a value of $C_\ell = 2.37$. In the present work for a value of $k_v = 0.37$, we obtain $C_\ell = 2.25$.

Numerical Solution

The approach followed in the present work is based on a cell-centered finite volume time marching formulation. Space and time discretizations are separated by using the method of lines, thus reducing the system of discretized equations to a system of ordinary differential equations. The inviscid flux is computed with a cell-centered approximation that satisfies consistency and conservation. The viscous flux is evaluated by means of Gauss theorem and a cell-center formulation. An adaptive dissipation flux, which ensures a total variation diminishing character of the scheme across shocks,[17] is added to inhibit spurious oscillations and avoid unphysical solutions.

For turbulent flows, the system of governing equations is stiff due to the disparity between the turbulence and fluid-dynamic time scales. Therefore, the time integration requires, in principle, an extremely small time step. To reduce the stiffness, we have introduced a precondition matrix $\boldsymbol{P}$ (that has the effect of scaling all of the characteristic times to the same order), which is related to the Jacobian of the source term of the two-equation turbulence model. For computational efficiency, a partial Jacobian has been used, whereby the dependency of μ^t on ρk and $\rho\epsilon$ is neglected, and both the low Reynolds and the compressibility effects are treated explicitly.

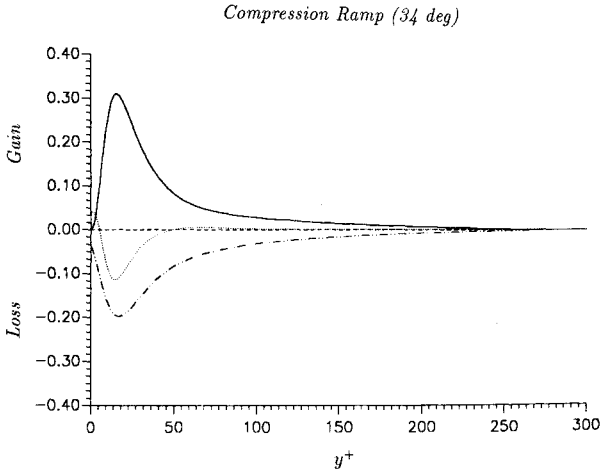

Fig. 7 Turbulence kinetic energy budget vs y^+ at $x/L = -0.5$, incompressible (—, P_k; - · -, ϵ; · · · ·, Diff.; - - -, Conv.).

The integration in time is performed by a five-stage Runge-Kutta algorithm, and the coefficients of the scheme are chosen to ensure high-frequency damping behavior.

Results

The model has been applied to simulate turbulent hypersonic flows over flat plates and compression ramps. The objective of the computations has been two-fold: 1) to assess the influence of the compressibility; and 2) to analyze the turbulence kinetic energy budget to get some physical insight on the shock-wave turbulence amplifying mechanism.

For all test cases, the turbulence kinetic energy and its dissipation rate are initialized in such a way as to have an initial turbulent viscosity of the same order of magnitude of the laminar viscosity. First-order extrapolation conditions are imposed at the outflow. At the wall, the turbulence kinetic energy and the normal derivative of the dissipation are set equal to zero. A different dissipation boundary condition, obtained from the asymptotic analysis, has also been used. However, the computed results are not affected by the different boundary condition treatment except for the dissipation distribution in a small portion of the laminar sublayer.

Test Case 1

The first test case corresponds to the flow over a flat plate at $M_\infty = 9.22$, unit Reynolds number $Re/m = 47 \times 10^6$, freestream temperature $T_\infty = 64.5$ K, wall temperature $T_w = 295$ K, and flat-plate length $L = 0.76$ m. For this test case, the velocity and Mach-number distributions have been measured by Coleman and Stollery.[23]

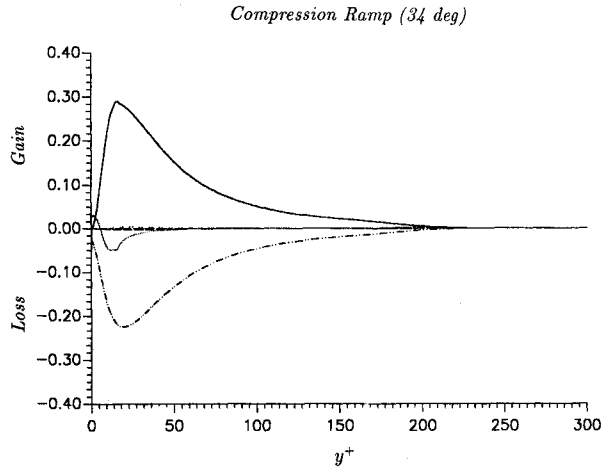

Fig. 8 Turbulence kinetic energy budget vs y^+ at $x/L = -0.5$, compressible (—, P_k; - · ·, ϵ; · · · ·, $\Pi_{c,1}$; -·-, $\Pi_{c,2}$; - - -, $\Pi_{c,3}$; · · ·, Diff.; - - -, Conv.).

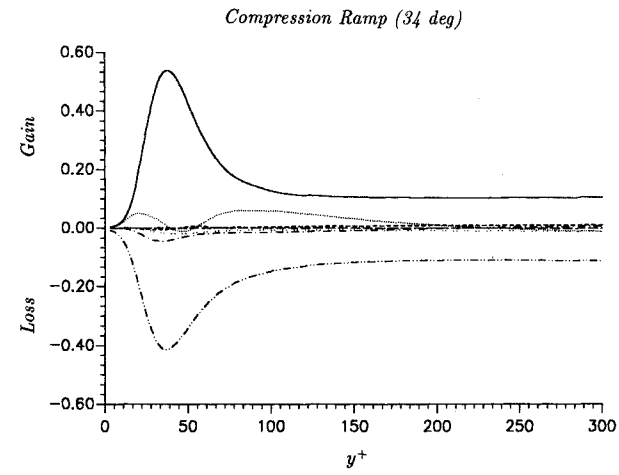

Fig. 9 Turbulence kinetic energy budget vs y^+ at peak heating location, compressible (—, P_k; - · ·, ϵ; · · · ·, $\Pi_{c,1}$; -·-, $\Pi_{c,2}$; - - -, $\Pi_{c,3}$; · · ·, Diff.; - - -, Conv.).

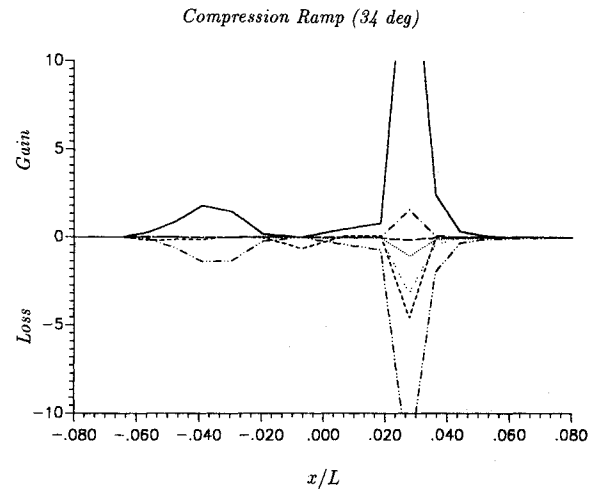

Fig. 10 Turbulence kinetic energy budget vs x/L at $y^+ = 400$, compressible (—, P_k; - · ·, ϵ; · · · ·, $\Pi_{c,1}$; -·-, $\Pi_{c,2}$; - - -, $\Pi_{c,3}$; · · ·, Diff.; - - -, Conv.).

All computations have been performed on a 256 × 64 mesh with normal nondimensional spacing ranging from $(\Delta y)_{\min} = 0.83 \times 10^{-5}$ to $(\Delta y)_{\max} = 0.17 \times 10^{-2}$, and aspect ratio (AR) varying between $(AR)_{\min} = 2.53$ and $(AR)_{\max} = 533$. A total of about 10 cells have been fitted in the laminar sublayer with the first cell located at $y^+ \simeq 0.1$. Two more computations have been performed to assess grids sensitivity on a coarser mesh (128 × 32) and a finer one (256 × 128).

Two computations are reported, corresponding to the complete compressible model of Eqs. (10) and (11) (referred to as compressible), and the simple variable-density extension, obtained by setting $\Pi_{c,i} = 0$ (referred to as incompressible). Figure 1 shows the velocity profile vs y/δ, where δ is the experimentally measured boundary-layer thickness ($\delta = 0.72$ cm). As the figure indicates, the effects of the compressibility corrections are negligible below $y/\delta \simeq 0.5$. However, in the outer region the compressible model yields a better agreement with the experimental data. This is mainly due to the dilatation-dissipation effects that contribute to reduce the turbulence kinetic energy, as well as the solenoidal dissipation. Consequently, the turbulent viscosity decreases and a somewhat flatter velocity profile is obtained. The comparison of the Mach-number distribution is also satisfactory as shown in Fig. 2. Some differences between the measured and the computed compressible values are observed: computed and measured results differ by 10–15%. The results also indicate that there are essentially no differences between the 256 × 64 and 256 × 128 grids. Moreover, the enforcement of the same spacing (only) near the wall yields the same results on all three grids for $y/\delta \leq 0.05$.

The turbulence kinetic energy budget (all terms are normalized by $\rho u_\tau^4/\nu_w$) shows a behavior typical of boundary-layer flows, and it is very similar to that reported by Zhang et al.,[11] So et al.,[24] Mansour et al.,[25] Galmes et al.,[26] and Rodi.[27] As observed from Fig. 3, turbulence is in equilibrium at distances $y^+ > 45$. The turbulence diffusion plays an important role in the layer $8 < y^+ < 45$. In the near wall region, the dissipation balances the molecular diffusion, and the production by mean velocity gradient is negligible. From Fig. 4 observe that the only compressibility effects come from the dilatation-dissipation; however, this contribution to the budget is small. Both the compressible and incompressible budgets show that the production has a maximum at the same distance from the wall. However, the compressible peak is reduced on account

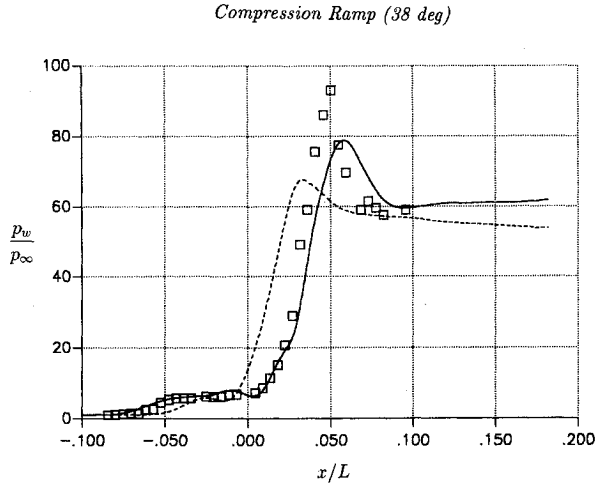

Fig. 11 Surface pressure vs x/L (□, Ref. 22; —, compressible; - - -, incompressible).

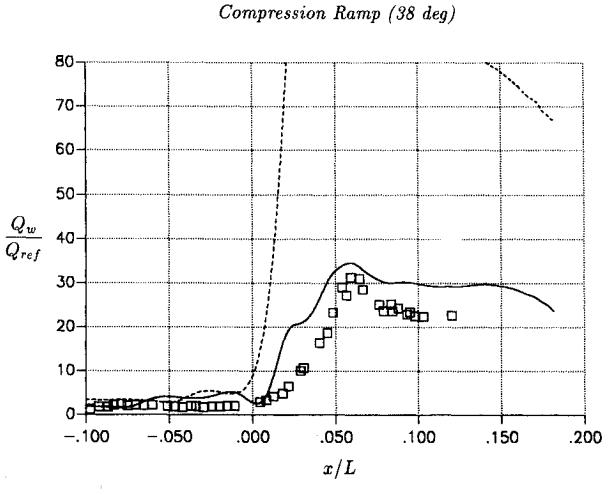

Fig. 12 Surface heat transfer vs x/L (□, Ref. 22; —, compressible; - - -, incompressible).

of the dilatation-dissipation which is also responsible for the reduction of the level of the turbulence kinetic energy within the boundary layer.

Test Case 2

The second test case corresponds to the flow over compression ramps at the same flow conditions of case 1. For this test case, the wall pressure and surface heat transfer distributions have been measured by Coleman and Stollery[23] and Elfstrom[28] for two different ramp angles ($\beta = 34$, 38 deg). All computations have been performed on a 176×98 mesh, and a total of about 10 cells have been fitted in the laminar sublayer with the first cell located at $y^+ \simeq 0.2$.

34-deg Compression Ramp

For this test case, two computations are reported, corresponding to the complete compressible model of Eqs. (10) and (11) and its incompressible version. The mesh normal nondimensional spacing ranges from $(\Delta y)_{\min} = 1.13 \times 10^{-5}$ to $(\Delta y)_{\max} = 1.19 \times 10^{-2}$, and aspect ratio varying between $(AR)_{\min} = 0.65$ and $(AR)_{\max} = 1182$.

The computed and measured wall pressure and surface heating are shown in Figs. 5 and 6. Both the incompressible and compressible models underpredict the peak pressure and overpredict the peak heating (a variable turbulent Prandtl number may contribute to reduce the overshoot in the heat transfer prediction). The computed results show that the compressible model yields adequate prediction of the plateau pressure, even though it yields a separation extent greater than the measured one. However, the recompression past the reattachment shock agrees well with the experimental measurements. On the other hand, the incompressible model yields a very high heating rate ($Q_w/Q_{\text{ref}} \simeq 120$; $Q_{\text{ref}} = 6.29\ \text{Wcm}^{-2}$), even though the pressure distribution is in a better agreement with the experiments.

Figures 7–9 show the turbulence kinetic energy budget at two different locations corresponding to 1) the flat plate midsection $x/L = -0.5$ (the origin of the axis being at the corner) and 2) the peak heating location. Before separation, the budget has a behavior typical of flat-plate flows, as Figs. 7 and 8 show. Moreover, the compressibility effects are rather negligible. The main differences between the compressible and incompressible budgets amount to a slight reduction of the solenoidal dissipation at the wall. Furthermore, within the layer of maximum turbulence kinetic energy production, the incompressible diffusion contribution is about twice the compressible one.

Figure 9 shows the effects of the reattachment shock amplifying mechanism at the peak heating location. It is interesting to notice that the diffusion contribution changes sign upstream and downstream of the shock, thus contributing to the turbulence kinetic energy amplification. The "Favre" and pressure-dilatation contributions are not negligible for $y^+ > 30$, and the dilatation-dissipation is equally important. Moreover, an asymptotic behavior is observed for $y^+ > 100$. A similar behavior is observed in the incompressible case. However, the maximum of the turbulence amplifying mechanism is found to occur closer to the wall [at $y^+ \simeq \mathcal{O}(10)$], which explains the extremely high value of the peak heating in the incompressible case. Within the recirculation bubble it is found that, due to the strong streamline curvature effects, production is not balanced by dissipation. The maximum of the production occurs at $y^+ = \mathcal{O}(300\text{–}400)$ where the amplifying mechanism due to the separation and reattachment shocks are important.

To further understand such a mechanism, the turbulence kinetic energy budget is plotted in Fig. 10 vs x/L at $y^+ = 400$ where x has to be intended as the streamwise direction. The figure shows the occurrences of two peaks corresponding to the separation and reattachment shocks. However, the effects of the latter are stronger. The pressure-dilatation and the "Favre" contributions are not negligible, and are of the same order of the diffusion and convection. Moreover, the budget shows that the production by mean velocity gradients and the "Favre" term are alleviated by the pressure-dilatation contribution that acts as a sink. This explains why in the incompress-

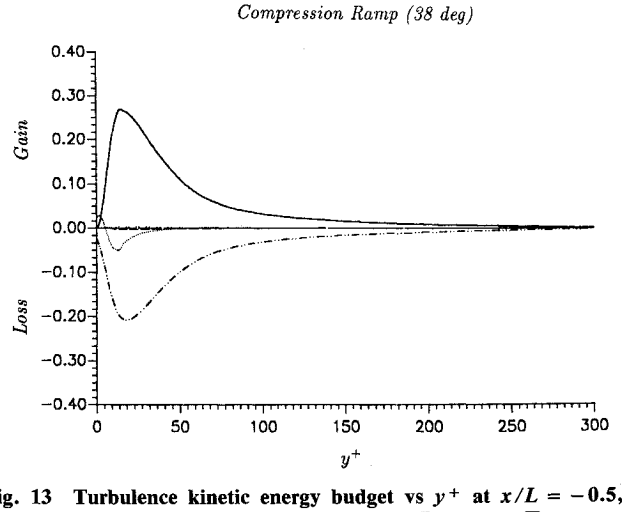

Fig. 13 Turbulence kinetic energy budget vs y^+ at $x/L = -0.5$, compressible (—, P_k; - · -, ϵ; · · · · , $\Pi_{c,1}$; -·-, $\Pi_{c,2}$; - - -, $\Pi_{c,3}$; · · ·, Diff.; - - -, Conv.).

ible case, having neglected such contributions, the peak heating value is greater than the compressible one.

38-deg Compression Ramp

For this test case, two computations are reported, corresponding to the compressible model of Eqs. (10) and (11), and its incompressible version. The mesh normal nondimensional spacing ranges from $(\Delta y)_{\min} = 9.33 \times 10^{-6}$ to $(\Delta y)_{\max} = 9.47 \times 10^{-3}$, and aspect ratio varying between $(AR)_{\min} = 0.92$ and $(AR)_{\max} = 1505$.

The wall pressure and the surface heating are shown in Figs. 11 and 12. The results computed with the compressible and the incompressible models are compared with the experimental values of Coleman and Stollery.[23] Both models underpredict the peak pressure. The incompressible model yields a reduced separation extent and a faster recompression after reattachment, and, consequently, an extremely high value of the peak heating ($Q_w/Q_{\text{ref}} \simeq 125$; $Q_{\text{ref}} = 6.56\ \text{Wcm}^{-2}$), as also found by other authors.[16] The compressible model predicts overall a satisfactory agreement with the experiments, even though some discrepancies are noticeable in the heating rate distribution, particularly within the recirculation bubble.

Concerning the turbulence kinetic energy budget before separation, a behavior typical of flat-plate flows is observed at $x/L = -0.5$, as shown in Fig. 13, and the compressibility effects are found to be rather negligible as already found in the 34-deg case. The behavior at the peak heating location is also similar to that observed in the 34-deg case, as shown in Fig. 14 where the budget vs y^+ is reported. Within the recirculation bubble, turbulence is not in equilibrium, and the maximum of the production is displaced toward the outer region (compared to the 34-deg case), due to the larger extent of the bubble. The effects of the "Favre" and pressure-dilatation contributions on the turbulence amplification across the reattachment shock are evident from Fig. 15, where the turbulence kinetic energy budget is plotted vs x/L at $y^+ = 400$ (that corresponds approximately to the distance of maximum production). For this test case, the effects of the separation shock are rather spread out, affecting roughly the entire region between the separation point and the corner.

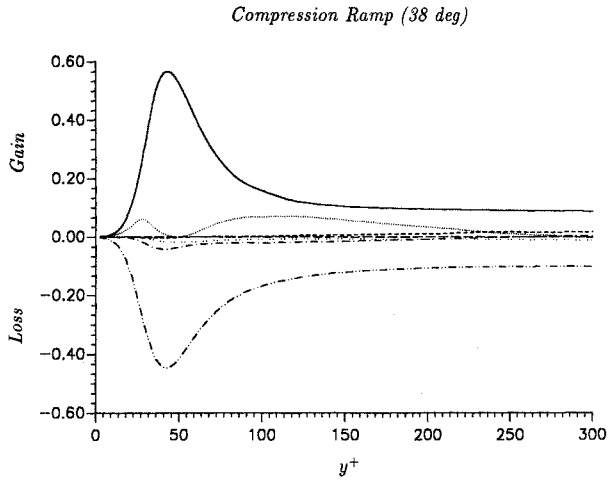

Fig. 14 Turbulence kinetic energy budget vs y^+ at peak heating location, compressible (—, P_k; - · -, ϵ; · · · ·, $\Pi_{c,1}$; -·-, $\Pi_{c,2}$; - - -, $\Pi_{c,3}$; · · ·, Diff.; - - -, Conv.).

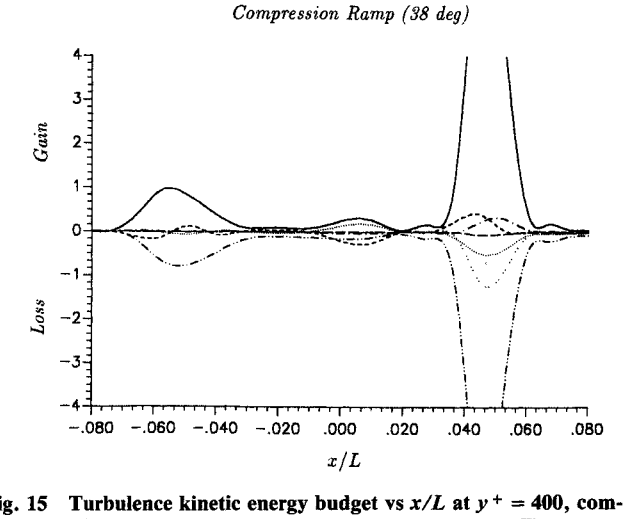

Fig. 15 Turbulence kinetic energy budget vs x/L at $y^+ = 400$, compressible (—, P_k; - · -, ϵ; · · · ·, $\Pi_{c,1}$; -·-, $\Pi_{c,2}$; - - -, $\Pi_{c,3}$; · · ·, Diff.; - - -, Conv.).

Conclusions

In the present work, a two-equation turbulence model has been developed and critically evaluated by extensive comparison with available experimental data that amount to velocity, Mach number, surface pressure, and heat transfer distributions. The model satisfies the near wall asymptotic behavior and is applicable in the presence of strong streamline curvature and adverse pressure gradients. The leading compressibility terms have been identified in the dilatation-dissipation, pressure-dilatation, and Favre velocity-mean pressure gradient contribution. The model also accounts for compressibility effects on the von Kármán's constant and on the turbulence length scale, which affects the heating rates. A study of hypersonic boundary-layer flows and shock-wave/boundary-layer interactions shows that the effects of compressibility depend on the flow complexity. Simple variable-density extension of incompressible two-equation models is shown to be inadequate in predicting the influence of compressibility even in simple flows. Overall the model here developed does predict adequately shock-wave/boundary-layer interactions as the comparison with the experiments indicates.

The analysis of the turbulence kinetic energy budget shows that across shocks diffusion contributes to the turbulence amplifying mechanism, and likewise for the "Favre" and pressure-dilatation contributions. In the absence of shock-induced separation, the dilatation contributions are negligible. For separated flows, the value of the peak heating depends strongly on the production of turbulence kinetic energy that peaks approximately at the location of maximum heat transfer. The pressure-dilatation contribution acts as a sink of turbulence kinetic energy and it counteracts the effects of the "Favre" contribution as well as the production by mean velocity gradients. As a consequence, if the compressibility effects are neglected the peak heating value is overestimated even more.

References

[1]Erlebacher, G., Hussaini, M. Y., Kreiss, O., and Sarkar, S., "The Analysis and Simulation of Compressible Turbulence," NASA CR-181997, Feb. 1990.

[2]Sarkar, S., Erlebacher, G., Hussaini, M. Y., and Kreiss, O., "The Analysis and Modeling Dilatational Terms in Compressible Turbulence," NASA CR-181959, Dec. 1989.

[3]Sarkar, S., "Modeling the Pressure-Dilatation Correlation," NASA CR-187566, May 1991.

[4]Zeman, O., "Dilatation Dissipation: The Concept and Application in Modeling Compressible Mixing Layer," *Physics of Fluids A,* Vol. 2, No. 2, 1990, pp. 178–188.

[5]Speziale, C. G., and Sarkar, S., "A Preliminary Compressible Second-Order Closure Model for High Speed Flows," NASA CR-181875, July 1989.

[6]Viegas, J. R., and Rubesin, M. W., "On Use of Wall Functions as Boundary Conditions for Two-Dimensional Separated Flows," AIAA Paper 85-0180, Jan. 1985.

[7]Patel, V. C., Rodi, W., and Scheuerer, G., "Turbulence Models for Near-Wall and Low Reynolds Number Flows: A Review," *AIAA Journal,* Vol. 23, No. 9, 1985, pp. 1308–1319.

[8]Speziale, C. G., Abid, R., and Anderson, E. C., "Critical Evaluation of Two-Equation Models for Near Wall Turbulence," *AIAA*

Journal, Vol. 30, No. 2, 1992, pp. 324–331.

[9]Abid, R., Speziale, G. C., and Thangam, S., "Application of a New k-τ Model to Near Wall Turbulent Flows," AIAA Paper 91-0614, Jan. 1991.

[10]Shih, T. H., "An Improved k-ϵ Model for Near-Wall Turbulence and Comparison with Direct Numerical Simulation," NASA TM-103221, Aug. 1990.

[11]Zhang, H. S., So, R. M. C., Speziale, C. G., and Lai, Y. G., "A Near Wall Two-Equation Model for Compressible Turbulent Flows," NASA CR-189565, Nov. 1991.

[12]Abid, R., "A Two-Equation Turbulence Model for Compressible Flows," AIAA Paper 91-1781, June 1991.

[13]Wilcox, D. C., "Progress in Hypersonic Turbulence Modeling," AIAA Paper 91-1785, June 1991.

[14]Viegas, J. R., Rubesin, M. W., "A Comparative Study of Several Compressibility Corrections to Turbulence Models Applied to High-Speed Shear Layers," AIAA Paper 91-1783, June 1991.

[15]Coakley, T. J., and Huang, P. G., "Turbulence Modeling for High Speed Flows," AIAA Paper 92-0436, Jan. 1992.

[16]Horstman, C. C., "Hypersonic Shock-Wave/Turbulent Boundary-Layer Interaction Flows: Experiment and Computation," AIAA Paper 91-1760, June 1991.

[17]Grasso, F., and Speziale, C. G., "Supersonic Flow Computations by Two-Equation Turbulence Modeling," AIAA Paper 89-1951, June 1989.

[18]Bagheri, N., Strataridakis, C. J., and White, B. R., "Measurements of Turbulent Boundary Layer Prandtl Numbers and Space-Time Temperature Correlations," *AIAA Journal,* Vol. 30, No. 1, 1992, pp. 35–42.

[19]Vandromme, D., "Contribution à la Modelisation et la Prediction d'Ecoulements Turbulents a masse Volumique Variable," Ph.D. Thesis, Université des Sciences et Techniques de Lille, Lille, France, 1983.

[20]Spalding, D. B., "Heat Transfer from Turbulent Separated Flows," *Journal of Fluid Mechanics,* Vol. 27, Pt. 1, Jan. 1967, pp. 97–109.

[21]Marvin, J. G., and Coakley, T. J., "Turbulence Modeling for Hypersonics Flows," The Second Joint Europe/U.S. Short Course in Hypersonics, Colorado Springs, CO, Jan. 1989.

[22]Settles, G. S., Dodson, L. J., "Hypersonic Shock/Boundary Layer Interaction Database," NASA CR-177577, April 1991.

[23]Coleman, G. T., and Stollery, J. L., "Heat Transfer from Hypersonic Turbulent Flow at a Wedge Compression Corner," *Journal of Fluid Mechanics,* Vol. 56, Pt. 4, 1972, pp. 741–752.

[24]So, R. M. C., Zhang, H. S., and Speziale, C. G., "Near-Wall Modeling of the Dissipation-Rate Equation," *AIAA Journal,* Vol. 29, No. 12, 1991, pp. 2069–2076.

[25]Mansour, N. N., Kim, J., and Moin, P., "Reynolds-Stress and Dissipation-Rate Budgets in a Turbulent Channel Flow," *Journal of Fluid Mechanics,* Vol. 194, Sept. 1988, pp. 15–44.

[26]Galmes, J. M., Dussauge, J. P., and Dekeyser, I., "Couches-Limites Turbulentes Supersoniques Soumises à un Gradient de Pression: Calcul à l'aide d'un modèle k-ϵ," Journal de Mécanique Théorique et Appliquée, Vol. 2, No. 4, 1983, pp. 539–558.

[27]Rodi, W., "Experience with Two-Layer Models Combining the k-ϵ Model with a One-Equation Model Near the Wall," AIAA Paper 91-0216, Jan. 1991.

[28]Elfstrom, G. M., "Turbulent Hypersonic Flow at a Wedge-Compression Corner," *Journal of Fluid Mechanics,* Vol. 53, Pt. 1, 1972, pp. 113–127.